Ultrasound in Medicine & Biology 51 (2025) 543–550

Contents lists available at ScienceDirect

Ultrasound in Medicine & Biology

journal homepage: www.elsevier.com/locate/ultrasmedbio

Original Contribution

Automatic Segmentation of Sylvian Fissure in Brain Ultrasound Images of Pre-Term Infants Using Deep Learning Models

María Regalado [a,b], Nuria Carreras [b], Christian Mata [b,c], Arnau Oliver [a,*], Xavier Lladó [a], Thais Agut [b]

[a] Research Institute of Computer Vision and Robotics, University of Girona, Girona, Spain
[b] Neonatal Brain Research Group, Institut de Recerca Sant Joan de Déu, Barcelona, Spain
[c] Universitat Politècnica de Barcelona, Barcelona, Spain

ARTICLE INFO

Keywords:
Pre-term infants
Brain sulci
Sylvian fissure
Segmentation
Deep learning
Ultrasonic imaging

ABSTRACT

Objective: Segmentation of brain sulci in pre-term infants is crucial for monitoring their development. While magnetic resonance imaging has been used for this purpose, cranial ultrasound (cUS) is the primary imaging technique used in clinical practice. Here, we present the first study aiming to automate brain sulci segmentation in pre-term infants using ultrasound images.

Methods: Our study focused on segmentation of the Sylvian fissure in a single cUS plane (C3), although this approach could be extended to other sulci and planes. We evaluated the performance of deep learning models, specifically U-Net and ResU-Net, in automating the segmentation process in two scenarios. First, we conducted cross-validation on images acquired from the same ultrasound machine. Second, we applied fine-tuning techniques to adapt the models to images acquired from different vendors.

Results: The ResU-Net approach achieved Dice and Sensitivity scores of 0.777 and 0.784, respectively, in the cross-validation experiment. When applied to external datasets, results varied based on similarity to the training images. Similar images yielded comparable results, while different images showed a drop in performance. Additionally, this study highlighted the advantages of ResU-Net over U-Net, suggesting that residual connections enhance the model's ability to learn and represent complex anatomical structures.

Conclusion: This study demonstrated the feasibility of using deep learning models to automatically segment the Sylvian fissure in cUS images. Accurate sonographic characterisation of cerebral sulci can improve the understanding of brain development and aid in identifying infants with different developmental trajectories, potentially impacting later functional outcomes.

Introduction

In the second half of pregnancy, the fetal brain goes through major developmental processes. Cerebral volume increases sixfold from weeks 21 to 38 of gestational age (wGA) and the smooth surface of the fetal brain undergoes a folding process that gives rise to the cerebral sulci and gyri [1]. This gyrification process takes place in a chronologically predictable manner, and at the end of gestation the distinctive convoluted pattern of the human brain is already perceptible. This folding process shows fast progression from 25 to 35 wGA and starts to decline after term birth [2]. If we consider that premature birth can happen as early as 22–23 wGA, the importance of the first weeks of life for these infants becomes apparent. Premature infant brain development presents a unique challenge to clinicians and researchers, as its occurrence in extra-uterine conditions may impact brain maturation during a critical period of development. Up to 50% of very pre-term infants will show impaired neurological outcomes, and in a non-neglectable number of them brain damage is not identifiable using conventional neuroimaging studies [3]. Recent research suggests that brain dysmaturation may be the underlying substrate of some neurological deficits observed in children born pre-term. Information about ways to assess such dysmaturation is largely lacking and mostly limited to magnetic resonance imaging (MRI) studies [4,5].

It has been shown that specific brain sulci and gyri are related to functional development [6,7], and that pre-term infants show alterations in sulcal patterns [8–13]. However, spatiotemporal details on pre-term dysmaturation and its functional impact still harbour unresolved questions. The first step in being able to identify an altered folding process is to map the "normal" developing brain. For this reason, research regarding pre-term brain segmentation is becoming of particular interest

* Corresponding author. Research Institute of Computer Vision and Robotics, University of Girona, Campus Montilivi, Ed. P-IV17003, Girona, Catalunya, Spain
E-mail addresses: mregaladobernabe@gmail.com (M. Regalado), nuria.carrerasb@sjd.es (N. Carreras), christian.mata@upc.edu (C. Mata), aoliver@eia.udg.edu (A. Oliver), xavier.llado@udg.edu (X. Lladó), thais.agut@sjd.es (T. Agut).

https://doi.org/10.1016/j.ultrasmedbio.2024.11.016
Received 9 July 2024; Revised 20 September 2024; Accepted 15 November 2024

[14,15]. Most authors use MRI due to its high resolution, although it has inherent limitations for performing sequential studies. In contrast, cerebral ultrasound (cUS) is the most common imaging modality used in neonatal units due to ease of use in a sequential and cost-effective manner, although, as image quality is lower, the segmentation of structures becomes more challenging. However, the possibility of performing sequential examinations makes it of great use for studying the gyrification process in pre-term infants *in vivo*.

To address this issue, we aimed to generate a weekly atlas of brain maturation using cUS images. In order to accomplish this, segmentation of the main cerebral sulci was required. During the first attempt at atlas generation, a semi-automatic sulci segmentation tool was developed [16]. This tool employed traditional image-processing methods such as K-means, active contour and thresholding to perform the segmentation task. However, the process of segmenting the different sulci using this application still required significant manual intervention, making it time-consuming and error prone. In addition, recent developments in deep learning algorithms have surpassed the accuracy of traditional image-processing algorithms.

This study presents the first attempt at segmenting brain sulci and gyri in the cUS images of pre-term infants using deep learning-based segmentation algorithms. To test the feasibility of our approach, we focused on a single sulcus, the Sylvian fissure, in a single cUS plane (C3). Figure 1a shows an example of a cUS image of the C3 plane of a pre-term newborn, while Figure 1b schematically shows the principal sulcus.

To automate segmentation of the Sylvian fissure, we introduced and analysed different approaches for segmentation, namely the well-known U-Net [17] and ResU-Net [18] models. These methods were selected due to their proven effectiveness and robustness in medical image segmentation, particularly in applications requiring high precision at pixel level, including ultrasound images [19–21]. U-Net in particular is known for its ability to handle small datasets, which is often a constraint in medical imaging studies, while maintaining reliable performance. Although more recent architectures have been developed, the primary goal of this work was to address a novel problem, *i.e.*, brain sulci segmentation in ultrasound images, which had not been previously explored. Given the complexity and novelty of this task, we prioritised the use of well-established methods with a track record of success in similar medical imaging challenges to ensure accuracy and interpretability.

These techniques were evaluated quantitatively with a dataset created in this study and validated by two clinical experts in the field. Furthermore, images external to the original dataset were segmented to evaluate generalisation of the models on a dataset different from the original one; in particular, a dataset with images of pre-term newborn brains taken with other US scanners. Fine-tuning techniques were used to segment these new images, providing a comparative study to evaluate the performance of the different configurations used to segment the new images.

Materials and methods

Database

Subjects originated from a prospective, longitudinal cohort of pre-term infants born in two tertiary neonatal units. Pre-term infants born before 32 weeks of gestation between January 2019 and June 2020, without suspicion of genetic disease or major malformations, were eligible. The original database was constructed from 146 infants, and after exclusion of 15 infants with intrauterine growth restriction, 44 from multiple gestation, 4 with relevant brain injury in the first exam and 10 with a C3 plane that did not pass image quality control (the Sylvian fissure was not identifiable in the image), 73 subjects were included for development of the automatic segmentation model. Written consent after oral and written information was provided was obtained from all subjects' parents. The study was approved by the ethical committee of the participant hospital.

Ultrasound study protocol included a scan within the first 3 days of life, followed by weekly scans until discharge or 40 weeks' gestational age. For this study, we included all scans performed before 32 weeks of post-menstrual age. Hence, the final number of C3 planes used in this work was 240, as each subject may have had several ultrasound scans. All ultrasound images were obtained by a neonatologist with experience in the field (N.C.) using a My Lab Alpha (Esaote, Genova, Italy) microconvex probe (4–9 MHz), properly anonymised and stored digitally.

External dataset

In addition to the previous dataset, another dataset of images was used to evaluate the generalisation of the models. This new dataset consisted of 36 new C3 planes of pre-term infants born from 24 to 31 wGA. These images were taken using Siemens Acuson S3000 and Canon Applio i700 ultrasound scanners as opposed to the original images, which were taken with an Esaote ultrasound scanner.

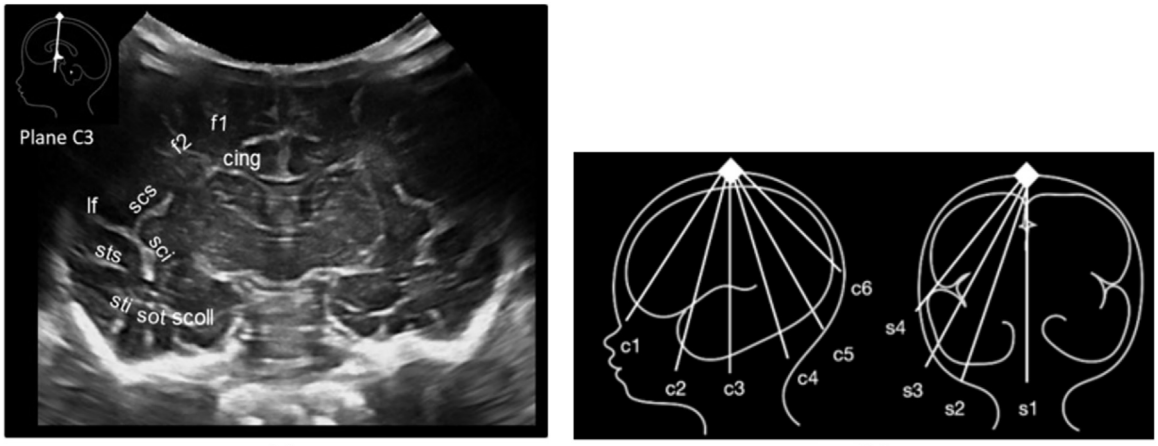

Figure 1. (a) C3 cranial ultrasound plane of a pre-term infant showing the main principal sulcus. f1, superior frontal sulcus; f2, inferior frontal sulcus; cing, cingulate sulcus; lf, lateral or Sylvian fissure; scs, sulcus circularis superior; sci, sulcus circularis inferior; sts, superior temporal sulcus; sti, inferior temporal sulcus; sot, sulcus occipitotemporalis; scoll, sulcus collateralis. (b) Anatomic references for each plane: c1, orbital border; c2, sphenoidal ridge; c3, foramina of Monro and third ventricle; c4, fourth ventricle; c5, choroid plexus; c6, visibility of parieto-occipital sulcus in the inferior tier of the image; s1, midsagittal; s2, lateral ventricles; s3, lateral fissure; s4, lateral fissure at the bottom of the image.

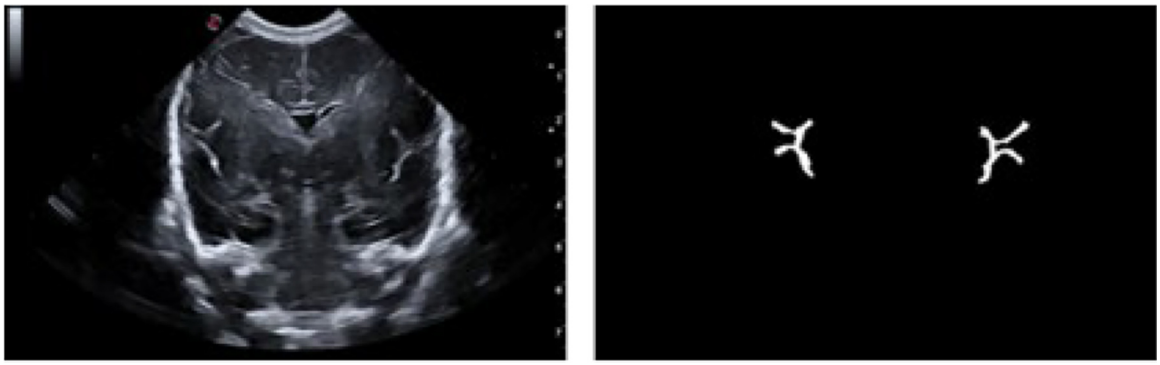

Figure 2. Example of the ultrasound image (*left*) and its corresponding binary mask of Sylvian sulcus segmentation (*right*).

Data pre-processing

Before segmentation of the Sylvian fissure, pre-processing of the images was carried out. The original images provided by the clinicians were 800 × 1068 pixels in size, and including labels and tags. During the pre-processing stage the images were cropped to eliminate those tags and labels, allowing the segmentation algorithm to focus only on the neonatal brain. The result of this step produced images of 550 × 868 pixel size.

Ground truth data annotation

In order to both perform training of the deep learning-based segmentation algorithms and evaluate the result of the algorithms, we required manual segmentation of the Sylvian sulcus. To create the manual segmentation masks for the 240 images, we used the MATLAB graphical interface "Image Segmenter" (Image Processing Toolbox, v. R2022b, The MathWorks Inc., MA, USA). In this interface there is a tool called Draw ROIs that allows the creation of regions of interest. All segmentations were validated by two expert clinicians. Figure 2 shows an example of the ultrasound and its corresponding binary mask. Notice that the Sylvian sulcus may appear in both right and left hemispheres (although in some images only one of the two is visible in the image, as we have shown in the results section).

Methodology

Deep learning architectures. To perform the segmentation task, we explored the use of both U-Net and ResU-Net architectures. The U-Net model has a two-stage U-shaped architecture, with the descending stage called the encoder and the ascending stage called the decoder. In the encoder part, convolutions and max-pooling operations are applied to extract features from the image at the same time as spatial resolution is reduced, allowing for context capturing. In the decoder stage, transposed convolutions and feature concatenation are used to gradually increase the spatial resolution and generate a detailed output and precise localisation of the image mask. The encoder and decoder parts are joined by the bottleneck, with the bottom transition layer compressing information before passing it to the expanding path. Skip connections link corresponding layers in the encoder and decoder paths, ensuring the transfer of fine-grained details for accurate segmentation.

The ResU-Net model is a variant of the U-Net model that uses residual connections to improve gradient propagation during training. These residual blocks are used in both encoder and decoder parts, as well as in the bottleneck. These residual blocks allow information to flow directly through connection hops, avoiding degradation problems during deep network training. Each residual block in ResU-Net consists of two convolutional layers followed by normalisation and activation layers. In addition to the residual blocks, there is another difference between the U-Net and the ResU-Net models implemented in our work. While the U-Net model uses a ReLU activation layer in the final output, the ResU-Net model uses a Softmax activation layer in the channel dimension. This allows generation of a segmentation output with a smoother probability distribution instead of simply a binary mask. In summary, the ResU-Net model allows for more parameters and layers compared with the classical U-Net model. This is due to the introduction of residual blocks, which allow the capture of more complex features and higher level representations.

Figure 3 shows a scheme of the U-Net and ResU-Net models used in this study, detailing the number of levels and the size of each convolutional step.

Fine-tuning. It is well known that deep learning algorithms show a drop in performance when testing images acquired with a different scanner machine to the one(s) used in training. Fine-tuning strategies help to adapt a pre-trained model to the specific characteristics and nuances of the new data domain. Fine-tuning also allows the model to adjust its parameters through continued training on the new data, aligning its representations and predictions with the target dataset. This process enables the model to leverage its prior knowledge while also accommodating the idiosyncrasies of the specific data it will be applied to, ultimately enhancing its performance, generalisation and applicability to the task at hand.

In this work we explored the use of fine-tuning our previous models trained with the in-house data and evaluated their performance using the external dataset acquired with different scanners. For the fine-tuning phase, the full U-Net/ResU-Net models were retrained using a small subset of images from the second dataset. This process involved adjusting the pre-trained model, which was initially trained on a large dataset, with a limited number of new examples. To facilitate gradual and stable adaptation, the learning rate was reduced by a factor of 10 during this phase, where all the network parameters were updated. This approach allowed effective fine-tuning of the model to better align with the new dataset while preserving knowledge gained from the initial training. The combination of using a smaller dataset and a lower learning rate ensured precise adjustments and maintained stability throughout the training process.

Evaluation. The metrics used for evaluating the results of Sylvian fissure segmentation were the dice similarity co-efficient (DSC) and sensitivity. DSC measured the similarity between predicted and ground truth segmentations, indicating how well the model captures the overall shape and overlap. Sensitivity evaluated the proportion of actual positives correctly identified by the model, reflecting its ability to detect true segmented pixels.

Paired t-tests were done to compute the statistical significance of the results. A p-value less than 0.05 was considered significant.

Implementation details

Both models were trained individually. The training process involved running the models for a maximum of 100 epochs, with a patience of 10

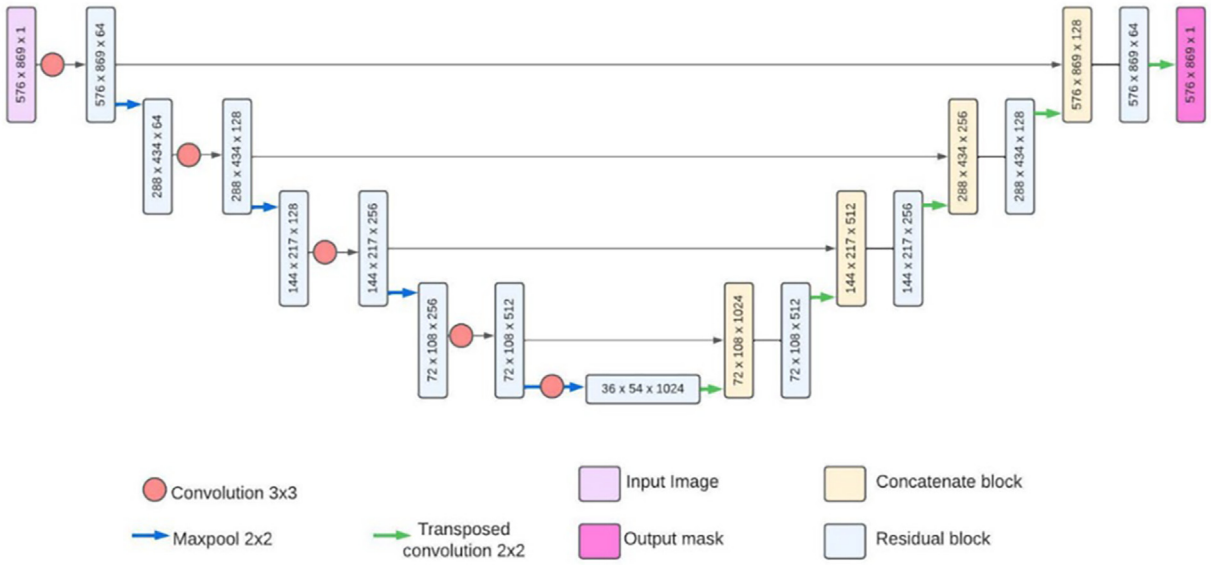

Figure 3. U-Net and ResU-Net architectures used for Sylvian fissure segmentation in pre-term infants. The difference between both architectures is the use or not of residual blocks in the grey-coloured blocks.

epochs. The learning rate for optimisation was set at 0.0001 using the Adam optimiser. To implement the models the PyTorch Lightning library was utilised, with PyTorch serving as the underlying framework. All experiments were conducted on a server equipped with a single NVIDIA GeForce GTX 1080 GPU.

Experimental evaluation

In-house dataset

For evaluating the performance of deep learning methods, we trained the nets using a cross-validation approach and validated them in an independent set. We therefore divided the dataset into two disjointed parts of 204 images for training and 36 for testing. Subsequently, we divided the training data into 6 different folds, each containing 34 images. In the cross-validation strategy, 5 folds where used for training and the remaining fold was used for validation. This process was repeated 6 times, each time using a different part for validation. Finally, the results were averaged to obtain an overall evaluation of the model's performance. Notice that we ensured that images of the same patient were assigned to the same partition.

To provide an example of the training results, Table 1 presents the results obtained by the ResU-Net model during the six-fold cross-validation of each fold. We can see that the results are similar and stable during each fold, therefore suggesting that the model was not heavily overfitted to any specific subset of the training data, and its predictive ability was relatively uniform across the entire dataset.

Table 1
Results of the six-fold cross-validation when ResU-Net model is tested.

	DSC	Sensitivity
Fold 1	0.791 ± 0.076	0.775 ± 0.101
Fold 2	0.774 ± 0.070	0.783 ± 0.085
Fold 3	0.793 ± 0.073	0.799 ± 0.088
Fold 4	0.786 ± 0.075	0.777 ± 0.100
Fold 5	0.792 ± 0.069	0.790 ± 0.078
Fold 6	0.774 ± 0.070	0.783 ± 0.085

Each fold has 34 testing images.
DSC, dice similarity co-efficient.

Table 2
Results of the U-Net and ResU-Net models when testing the independent dataset

	U-Net		ResU-Net	
	DSC	Sensitivity	DSC	Sensitivity
Independent test	0.710 ± 0.079	0.706 ± 0. 079	0.777 ± 0.072	0.784 ± 0. 090

DSC, dice similarity co-efficient.

Table 2 shows the results obtained for both U-Net and ResU-Net models when testing the deep learning architectures in the independent dataset of 36 images. Notice that testing the performance in a dataset not used during training was critical for unbiased validation. In general, the results showed good performance, although the ResU-Net results were significantly better ($p = 0.017$) than that obtained by U-Net. In addition, in both models we obtained similar results for both DSC and sensitivity. This indicates that our model demonstrated a good balance between detecting true positives and the overall accuracy of the segmentation, showing that the model not only successfully identified most of the positive areas (high sensitivity), but also that these predicted areas closely matched the actual areas (high DSC). In other words, the model accurately segmented in terms of both coverage and spatial precision.

Figure 4 shows some qualitative results. The first column showcases the original pre-processed images, while the second column shows a zoomed-in view of the original plane focused on the region of interest, the Sylvian fissure. The third column shows the ground truth, while the fourth and five columns present the automated Sylvian fissure segmentation obtained by U-Net and ResU-Net, respectively. Both algorithms were able to detect the Sylvian fissure in all images, although ResU-Net achieved more consistent segmentation. However, in Figure 4f both algorithms produced a false positive at the location where the Sylvian fissure should have been but did not appear in the original image.

External dataset

In this experiment we explored the ability of the algorithm to segment similar images acquired with a different imaging scanner. Using a testing set of seven different images, we performed three different tests:

- Segmenting the new images directly with the ResU-Net model trained with the in-house dataset;

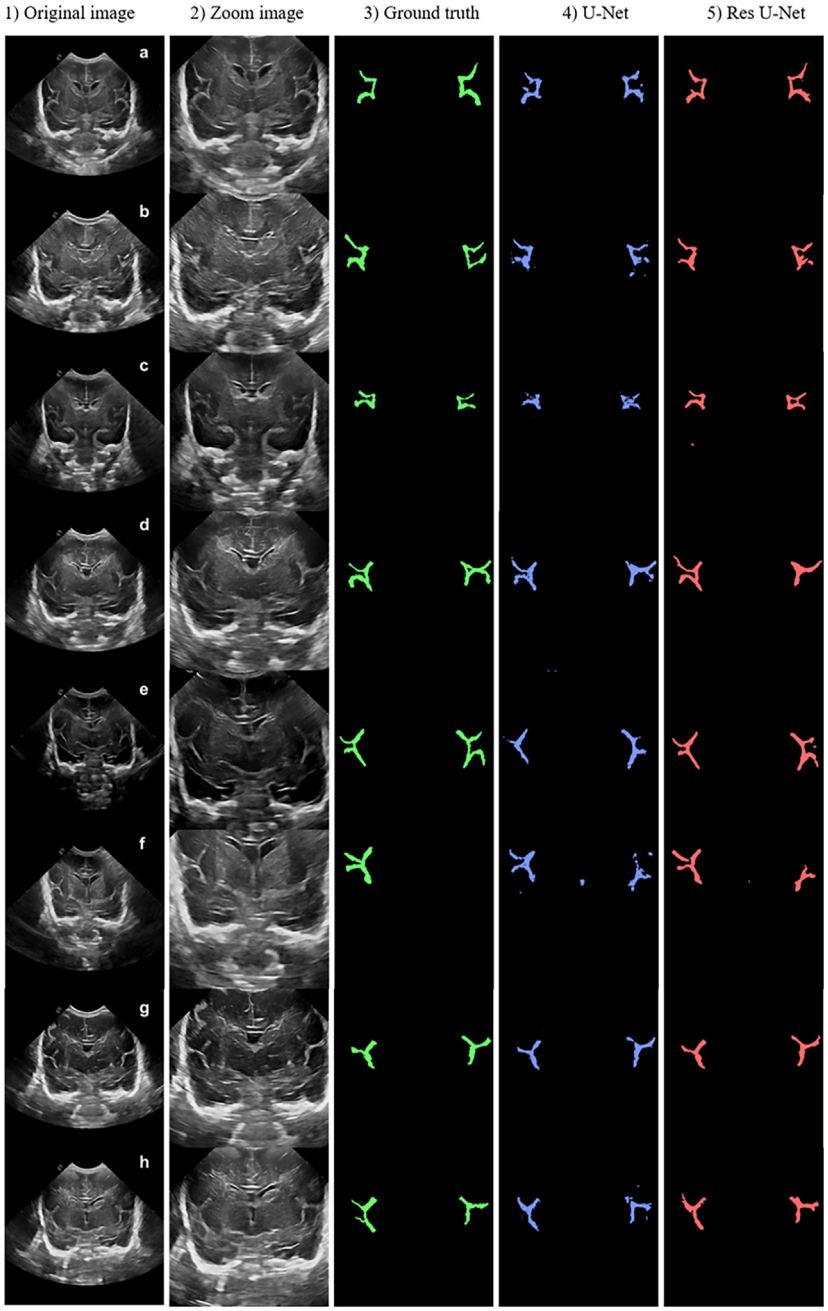

Figure 4. Example of Sylvian fissure segmentation of eight different cranial ultrasound images acquired using the same machine as the images used for training the deep learning models.

- Fine-tuning the models using a small part of the new images;
- Training from scratch a new model using most of the new images (29 images, excluding the testing ones).

Table 3 shows the results of the three experiments, again in terms of DSC and sensitivity. When directly using the model trained with the in-house dataset, the results indicated that the model was able to detect the region where the Sylvian fissure was located in almost all images (except image 2). However, in some images sensitivity was significantly lower than DSC, indicating a larger number of false positives. These results are also graphically shown in Figure 5, where we can see that in some cases the resulting segmentation was rather inadequate, leading to poorer outcomes when compared with segmentations achieved using the original dataset.

The results obtained while fine-tuning the previous model and while retraining the full ResU-Net are also shown in Table 3. In all cases, fine-tuning the model or retraining it achieved better performance than the direct test. In addition, the fine-tuning strategy obtained better results than retraining all the models, likely due to the small number of images used during retraining. The superior performance of the fine-tuning strategy can be qualitatively seen in Figure 5. Interestingly, the algorithms were able to detect that there was only one Sylvian fissure visible in Image 3.

Regarding performance based on the vending machine, the results obtained with images acquired using the Siemens machine were much better than those acquired from the Canon machine. In Figure 5, we can see that the appearance of the Siemens images were more similar to the training images (Fig. 4) than the Canon images, which had lower brightness and a different field of view. In both cases, however, the fine-tuning strategy allowed us to improve segmentation performance.

Discussion

In this work we demonstrated the feasibility of deep learning approaches for brain sulci segmentation in ultrasound images used in

Table 3
Results obtained by the ResU-Net model when testing the external dataset.

	Direct test		Fine-tuning		Retraining from scratch	
	DSC	Sensitivity	DSC	Sensitivity	DSC	Sensitivity
Image 1 (Canon)	0.491	0.369	0.706	0.652	0.505	0.377
Image 2 (Canon)	0.021	0.015	0.452	0.331	0.337	0.234
Image 3 (Canon)	0.603	0.693	0.771	0.767	0.631	0.528
Image 4 (Canon)	0.289	0.226	0.605	0.487	0.615	0.501
Image 5 (Siemens)	0.566	0.426	0.726	0.638	0.649	0.613
Image 6 (Siemens)	0.704	0.638	0.762	0.719	0.710	0.623
Image 7 (Siemens)	0.459	0.396	0.643	0.606	0.543	0.594

DSC, dice similarity co-efficient.

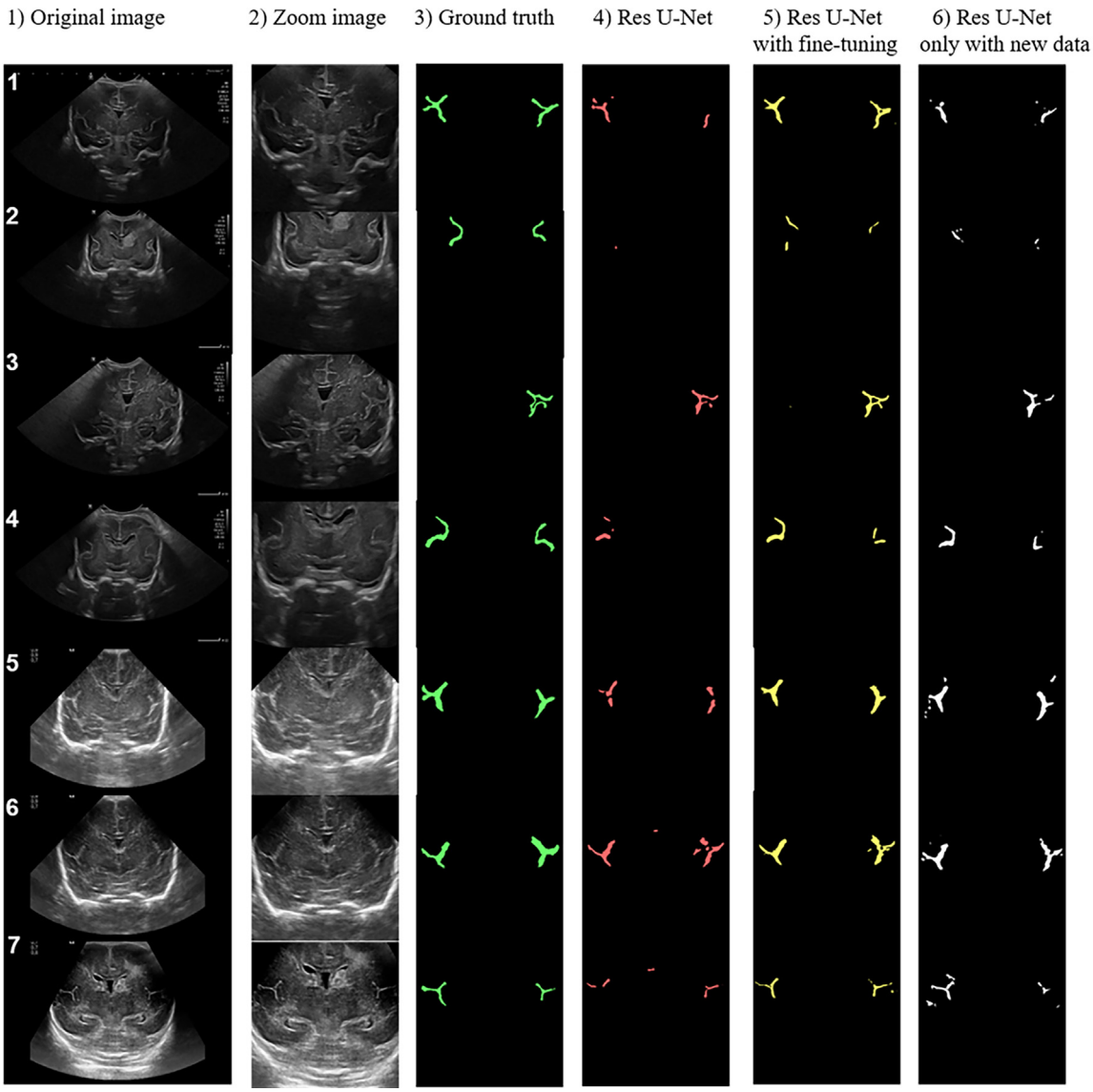

Figure 5. Segmentation results from external dataset images. Images 1–4: Canon scanner; images 5–7: Siemens scanner.

clinical practice as well as tested the use of U-Net and ResU-Net for this task. Both models demonstrated the ability to detect the Sylvian fissure structure, indicating that they were successful at capturing desired anatomical features. Figure 4 qualitatively shows the performance of both algorithms, obtaining correct segmentation results in almost all images.

However, the segmentations produced by ResU-Net appeared to be more continuous and smooth, indicating better preservation of the structural coherence of the Sylvian fissure. In contrast, U-Net segmentations exhibited more fragmented and irregular boundaries, which was reinforced by looking at the results of Table 2, where ResU-Net consistently obtained better DSC and sensitivity values in all images. These findings support the idea that incorporating residual connections in the U-Net architecture is able to improve the ability of the model to learn and represent complex anatomical structures with greater results.

Table 1 reaffirms these results, as it presents the outcomes of six-fold cross-validation using the ResU-Net model, showing robustness and consistently delivering accurate and reliable segmentations across the different folds. Furthermore, it is worth highlighting that ResU-Net demonstrated a reduced number of false-positive regions and detected fewer smaller regions that were incorrectly labelled as part of the Sylvian fissure. This indicates that ResU-Net has a better ability to discriminate and focus on accurately capturing the desired structure while minimising false detections.

In addition, we tested the generalisation results obtained when testing images acquired from different cUS vendors. Our results showed differing behaviour depending on the vendor. For the Siemens images, the obtained results were only slightly worse than those obtained when testing the same dataset. However, the results from the Canon images were definitively worse, and even failed to detect the Silvian sulcus in some images. By visually comparing the images, we noticed that images acquired using Canon ultrasound equipment were visually very different from the original dataset images compared with images acquired using the Siemens equipment.

To improve our results, retraining and fine-tuning strategies with additional images from the two vendors were employed. Fine-tuning strategies showed superior performance to retraining the models, likely due to the small amount of data. Thanks to the fine-tuning process, the algorithm successfully detected the position of the Sylvian fissure in all images and enhanced the segmentation of structures that were already well-segmented even without fine-tuning. We performed the fine-tuning experiment using different sets of images (1, 3, 5, 10, 20 and 29), and our results showed that from 10 images onward the network successfully adapted to the new data, yielding consistent outcomes with no statistically significant differences. However, when using fewer than 10 images, performance decreased. We also found that fine-tuning with a smaller subset of images mitigated the risk of catastrophic forgetting, preventing the model from overfitting to the new domains and preserving its performance in the original domain. Moreover, the improved computational efficiency achieved by reducing training time enabled us to refine the model without the need for extensive manual annotations. This approach is particularly relevant in scenarios where acquiring and annotating new data is difficult or expensive. Nevertheless, it is important to note that the segmentations still did not achieve the same level of accuracy as those obtained in images from the original dataset. In Image 2, the algorithm failed to segment the Sylvian fissure as a single uniform region and instead divided it into two separate regions. Additionally, small regions were detected that were not part of the ground truth. These findings indicate that there are remaining challenges in achieving optimal segmentations in these specific cases. Despite these limitations, the fine-tuning process proved to be effective at improving segmentations, enabling the algorithm to detect the position of the Sylvian fissure in all test images.

Segmenting the pre-term brain has gained increased interest in the last decade. Great advances have been made in the field using MRI, and segmentation of the sulci and gyri, as well as the quantification of properties such as tortuosity and depth, have become a reality in the research setting [22–24]. However, as far as we know, segmentation of cerebral sulci using ultrasound images has not been reported before. If we consider that there is a link between sulcal pattern and neurological function, and that the gyrification process takes place during the pre-term period, mapping the changing pre-term brain constitutes an opportunity for better definition of the spatiotemporal characteristics of brain gyrification to identify shape variants and assess how morphological characteristics affect function. Unlike MRI, cUS facilitates the frequency of exams required for this purpose.

Our research focused on the Sylvian fissure, which is one of the major and more characteristic sulci on the surface of the brain. Its conformation following frontal and temporal growth, covering the insular lobe, is unique regarding cerebral sulcal formation [25]. Two different areas can be distinguished related to the Sylvian fissure. External to it, the peri-Sylvian regions are involved in language function, including speech perception and production [26]. In the depths of the Sylvian fissure lies the insular cortex, which is partially responsible for sensorimotor, socioemotional and cognitive processing [27], all of which are functions commonly deficient in the pre-term population [28,29].

Moreover, morphological abnormalities of the Sylvian fissure may indicate post-migrational disorders such as polymicrogyria, which could be present in metabolic, infectious or genetic diseases [30]. Therefore, automatic segmentation could be useful for identifying pathological processes. Furthermore, enlargement of the Sylvian fissure may indicate increased subarachnoid spaces, which is a common feature in the longitudinal evolution of pre-term infants [31,32] and is often accompanied by microcephaly due to brain atrophy in some, as well as in the context of macrocephaly in others [33]. Enlarged subarachnoid spaces have been associated with poor outcomes in term and pre-term infants [33,34]. Hence, segmentation of the Sylvian fissure may allow the study of its morphology in relation to enlarged subarachnoid spaces and to investigate a possible association with neurological delays. Furthermore, structural asymmetries within the Sylvian fissure have been related to functional lateralisation in language processing [35,36].

The results of this study open the door to characterise brain-maturation trajectories in pre-term infants in an attempt to identify which kind of deviation from the standard pathway is linked to altered neurological functions. cUS appears to be a promising tool for complementing MRI data, offering the sequential information that is inevitably lacking from MRI studies.

We would like to remark that the segmentation methods employed in this study have demonstrated strong performance in the task of brain sulcal segmentation in ultrasound images. These architectures are well-established and widely recognised for their effectiveness in medical image segmentation tasks, providing reliable and interpretable results. However, it is important to acknowledge that these methods are not the most recent advances in the field of deep learning-based segmentation. While newer architectures such as transformer-based models or advanced attention mechanisms have emerged, our focus was on ensuring robust and interpretable segmentation in this novel application rather than prioritising the use of the latest algorithms. Future work may benefit from exploring these more modern approaches to potentially improve performance further.

Conclusion

In conclusion, this study demonstrated the feasibility of deep learning models for automatically segmenting the Sylvian fissure in cUS images. In addition, we showed the superiority of the ResU-Net model over the U-Net model with regard to accuracy. The outcome of this work contributes to the field of automated brain segmentation in pre-term infants and emphasises the importance of incorporating deep learning models with residual connections for accurate and reliable segmentations. Sonographic characterisation of the cerebral sulci may allow a better understanding of brain development as well as be useful for identifying infants with different trajectories of development, which could have an impact on later functional development.

Author contributions

M. Regalado: Methodology, Implementation, Data curation, Investigation, Formal analysis, Writing – original draft. N. Carreras: Data curation, Conceptualisation, Writing – review & editing. C. Mata: Methodology, Supervision, Conceptualisation. A. Oliver: Supervision, Investigation, Formal analysis, Writing – review & editing. X. Lladó: Supervision, Formal analysis, Writing – review & editing, Project administration. T. Agut: Data curation, Conceptualisation, Writing – review & editing, Project administration.

Data availability

Research data remains confidential and will not be shared.

Conflict of interest

The authors declare no competing interests.

Funding

This work was supported by grant no. PI18/00110 from the Instituto de Salud Carlos III, co-funded by the European Regional Development Fund.

References

[1] Mallela AN, Deng H, Bush A, Goldschmidt E. Different principles govern different scales of brain folding. Cereb Cortex 2020;30:4938–48. doi: 10.1093/cercor/bhaa086.
[2] Dubois J, Lefèvre J, Angleys H, Leroy F, Fischer C, Lebenberg J, et al. The dynamics of cortical folding waves and prematurity-related deviations revealed by spatial and spectral analysis of gyrification. Neuroimage 2019;185:934–46. doi: 10.1016/j.neuroimage.2018.03.005.
[3] Miller SP, Ferriero DM, Leonard C, Piecuch R, Glidden DV, Partridge JC, et al. Early brain injury in premature newborns detected with magnetic resonance imaging is associated with adverse early neurodevelopmental outcome. J Pediatr 2005;147:609–16. doi: 10.1016/j.jpeds.2005.06.033.
[4] Back SA, Miller SP. Brain injury in premature neonates: A primary cerebral dysmaturation disorder? Ann Neurol 2014;75:469–86. doi: 10.1002/ana.24132.
[5] Pittet MP, Vasung L, Hüppi PS, Merlini L. Newborns and preterm infants at term equivalent age: A semi-quantitative assessment of cerebral maturity. Neuroimage Clin 2019;24:102014. doi: 10.1016/j.nicl.2019.102014.
[6] Cachia A, Maschio ND, Borst G, Rosa PAD, Pallier C, Costa A, et al. Anterior cingulate cortex sulcation and its differential effects on conflict monitoring in bilinguals and monolinguals. Brain Lang 2017;175:57–63. doi: 10.1016/j.bandl.2017.09.005.
[7] Cachia A, Paillère-Martinot ML, Galinowski A, Januel D, de Beaurepaire R, Bellivier F, et al. Cortical folding abnormalities in schizophrenia patients with resistant auditory hallucinations. Neuroimage 2008;39:927–35. doi: 10.1016/j.neuroimage.2007.08.049.
[8] Eaton-Rosen Z, Scherrer B, Melbourne A, Ourselin S, Neil JJ, Warfield SK. Investigating the maturation of microstructure and radial orientation in the preterm human cortex with diffusion MRI. Neuroimage 2017;162:65–72. doi: 10.1016/j.neuroimage.2017.08.013.
[9] Kim H, Lepage C, Maheshwary R, Jeon S, Evans AC, Hess CP, et al. Neocivet: Towards accurate morphometry of neonatal gyrification and clinical applications in preterm newborns. Neuroimage 2016;138:28–42. doi: 10.1016/j.neuroimage.2016.05.034.
[10] Makropoulos A, Aljabar P, Wright R, Hüning B, Merchant N, Arichi T, et al. Regional growth and atlasing of the developing human brain. Neuroimage 2016;125:456–78. doi: 10.1016/j.neuroimage.2015.10.047.
[11] Mewes AU, Hüppi PS, Als H. Regional brain development in serial magnetic resonance imaging of low-risk preterm infants. Pediatrics 2006;118:23–33. doi: 10.1542/peds.2005-2675.
[12] Thompson DK, Kelly CE, Chen J, Beare R, Alexander B, Seal ML, et al. Characterisation of brain volume and microstructure at term-equivalent age in infants born across the gestational age spectrum. NeuroImage Clin 2019;21:101630. doi: 10.1016/j.nicl.2018.101630.
[13] Vandewouw MM, Young JM, Mossad SI, Sato J, Whyte HA, Shroff MM, et al. Mapping the neuroanatomical impact of very preterm birth across childhood. Hum Brain Mapp 2020;41:892–905. doi: 10.1002/hbm.24847.
[14] Engelhardt E, Inder TE, Alexopoulos D, Dierker DL, Hill J, Van Essen DC, et al. Regional impairments of cortical folding in premature infants. Ann Neurol 2015;77:154–62. doi: 10.1002/ana.24313.
[15] Ganella EP, Burnett A, Cheong J, Thompson D, Roberts G, Wood S, et al. Abnormalities in orbitofrontal cortex gyrification and mental health outcomes in adolescents born extremely preterm and/or at an extremely low birth weight. Hum Brain Mapp 2015;36:1138–50. doi: 10.1002/hbm.22692.
[16] Rabanaque D, Regalado M, Benítez R, Rabanaque S, Agut T, Carreras N, et al. Semi-automatic GUI platform to characterize brain development in preterm children using ultrasound images. J Imaging 2023;9:145. doi: 10.3390/jimaging9070145.
[17] Ronneberger O, Fischer P, Brox T. U-net: Convolutional networks for biomedical image segmentation. In: Navab N, Hornegger J, Wells W, Frangi A, editors. Medical image computing and computer-assisted intervention – MICCAI 2015. Cham: Springer; 2015. p. 234–41 Lecture Notes in Computer Science, vol. 9351. doi: 10.1007/978-3-319-24574-4_28.
[18] Xiao X, Lian S, Luo Z, Li S. Weighted res-unet for high-quality retina vessel segmentation. In: Paper presented at: 9th International Conference on Information Technology in Medicine and Education (ITME). October 19–21; 2018. p. Hangzhou, China327–31. doi: 10.1109/ITME.2018.00080.
[19] Zhang J, Jiang Z, Dong J, Hou Y, Liu B. Attention gate resu-net for automatic MRI brain tumor segmentation. IEEE Access 2020;8:58533–45. doi: 10.1109/ACCESS.2020.2983075.
[20] Martin M, Sciolla B, Sdika M, Quétin P, Delachartre P. Automatic segmentation and location learning of neonatal cerebral ventricles in 3D ultrasound data combining CNN and CPPN. Comput Biol Med 2021;131:104268. doi: 10.1016/j.compbiomed.2021.104268.
[21] Li C, Du R, Luo Q, Wang R, Ding X. A novel model of thyroid nodule segmentation for ultrasound images. Ultrasound Med Biol 2023;48:489–96. doi: 10.1016/j.ultrasmedbio.2022.09.017.
[22] Engelhardt E, Inder TE, Alexopoulos D, Dierker DL, Hill J, Van Essen D, et al. Regional impairments of cortical folding in premature infants. Ann Neurol 2015;77:154–62.
[23] Griffiths PD, Naidich TP, Fowkes M, Jarvis D. Sulcation and gyration patterns of the fetal brain mapped by surface models constructed from 3D MR image datasets. Neurographics 2018;8:124–9.
[24] Zhang Y, Inder TE, Neil JJ, Dierker DL, Alexopoulos D, Anderson PJ, et al. Cortical structural abnormalities in very preterm children at 7 years of age. Neuroimage 2015;109:469–79. doi: 10.1016/j.neuroimage.2015.01.049.
[25] Mallela AN, Deng H, Brisbin AK, Bush A, Goldschmidt E. Sylvian fissure development is linked to differential genetic expression in the pre-folded brain. Sci Rep 2020;10:14422. doi: 10.1038/s41598-020-71230-4.
[26] Catani M, Jones DK, Ffytche DH. Perisylvian language networks of the human brain. Ann Neurol 2005;57:8–16. doi: 10.1002/ana.20319.
[27] Uddin LQ, Nomi JS, Hébert-Seropian B, Ghaziri J, Boucher O. Structure and function of the human insula. J Clin Neurophysiol 2017;34:300–6. doi: 10.1097/WNP.0000000000000377.
[28] Vandormael C, Schoenhals L, Hüppi PS, Filippa M, Borradori Tolsa C, Montirosso R. Language in preterm born children: Atypical development and effects of early interventions on neuroplasticity. Neural Plast 2019;2019:5315431. doi: 10.1155/2019/5315431.
[29] Gray PH, Edwards DM, Hughes IP, Pritchard M. Social-emotional development in very preterm infants during early infancy. Early Hum Dev 2018;121:44–8. doi: 10.1016/j.earlhumdev.2018.05.015.
[30] Stutterd CA, Leventer RJ. Polymicrogyria: a common and heterogeneous malformation of cortical development. Am J Med Genet C Semin Med Genet 2014;166C:227–39. doi: 10.1002/ajmg.c.31334.
[31] Hammerl M, Zagler M, Zimmermann M, Griesmaier E, Janjic T, Gizewski ER, et al. Supratentorial brain metrics predict neurodevelopmental outcome in very preterm infants without brain injury at age 2 years. Neonatology 2020;117:287–93. doi: 10.1159/000507617.
[32] Horsch S, Skiöld B, Hallberg B, Nordell B, Nordell A, Mosskin M, et al. Cranial ultrasound and MRI at term age in extremely preterm infants. Arch Dis Child Fetal Neonatal Ed 2010;95:F310–4. doi: 10.1136/adc.2009.167882.
[33] Yum SK, Ah Im S, Seo YM, Sung K. Enlarged subarachnoid space on cranial ultrasound in preterm infants: neurodevelopmental implications. Sci Rep 2019;9:18050. doi: 10.1038/s41598-019-55604-x.
[34] Shen MD, Nordahl CW, Young GS, et al. Early brain enlargement and elevated extra-axial fluid in infants who develop autism spectrum disorder. Brain 2013;136:2825–35. doi: 10.1093/brain/awt166.
[35] De Vareilles H, Rivière D, Pascucci M, Sun ZY, Fischer C, Leroy F, et al. Exploring the emergence of morphological asymmetries around the brain's Sylvian fissure: a longitudinal study of shape variability in preterm infants. Cereb Cortex 2023;33:1877–88. doi: 10.1093/cercor/bhac347.
[36] Dubois J, Benders M, Lazeyras F, Borradori-Tolsa C, Leuchter RH, Mangin JF, et al. Structural asymmetries of perisylvian regions in the preterm newborn. Neuroimage 2010;52:32–42. doi: 10.1016/j.neuroimage.2010.03.043.